# Reading the interaction between vortex textures in a FORC diagram

**Alejandro Rivelles**[1], **Ana Parente**[2], **José L. Prieto**[1], **M. Mar Sanz-LLuch**[1], **Marco Maicas**[1] **and Manuel Abuín**[1]

[1]Instituto de Sistemas Optoelectrónicos y Microtecnología (ISOM), Universidad Politécnica de Madrid, 28040 Madrid, Spain

[2]Departamento de Física de Materiales, Facultad de Física, Universidad Complutense de Madrid, 28040 Madrid, Spain

E-mail: alejandro.rivelles.garcia@upm.es

**Abstract.** Many modern spintronic devices are based on large arrays of magnetic elements, where the interaction between them and their magnetic textures is often a key part of their performance. The experimental characterization of such arrays is challenging because it involves the knowledge of the magnetization process of millions of single elements over areas as large as several square millimetres. When the magnetic textures within the nano-elements interact between them, a characterization over the entire array can be complicated. Here we show how the interaction between vortex textures in adjacent ferromagnetic dots can be read in a First Order Reversal Curves (FORC) diagram. Using a 9 $mm^2$ array of ferromagnetic nanodots, we show how the shape and position of the prominent features in the FORC diagram describe the vortex nucleation and annihilation process. The intensity of these peaks gives information on how smooth the mobility of the vortex within the nanodot is. Also, by comparing the intensity of the main features, the FORC diagram is particularly sensitive to when the vortexes start interacting strongly with neighbouring vortexes. Micromagnetic simulations and measurements in arrays of different materials confirm our interpretation. With this work, we show the potential of the FORC diagram for disentangling the average magnetization process and the complex interactions between the different elements in a large array of nanostructures.

The peculiar properties of large arrays of magnetic nanoelements are becoming very relevant in modern magnetism. For instance, artificial spin-ice[1] has become very important in unveiling emergent phenomena[2,3,4], in high-frequency dynamics[5] and neuromorphic computing[6]. Nanoelements shaped as nanodisks, where a vortex is the most stable configuration, are the building blocks of many cutting-edge devices, such as low-noise magnetic sensors[7] or metasurfaces that allow the manipulation of microwaves and spin waves[8] for on-chip applications[9]. In addition, in the context of neuromorphic computing, interacting spin-torque nano-oscillators, where vortices are present, are among the most promising candidates for physical neural networks[10,11].

At the core of the rich functionality of the above-mentioned arrays of nanoelements, is the interaction between the magnetic textures (domain walls, vortex or skyrmions) between the individual elements of the array. The experimental characterization of these interactions is not trivial, as the imaging techniques either do not have enough resolution to image at the nanoscale or do not provide a wide field of view sufficient to image a significant proportion of the nanoelements. Often, the collective behaviour is inferred by a local image and micromagnetic simulations of a small portion of the array. In this context, as the arrays of nanoelements are quickly becoming more complex, it is pivotal to develop characterization techniques sensitive to the interaction between the magnetic textures in the whole collection of nanoelements, even if it is millimetres wide.

In this work, we show that First Order Reversal Curves (FORC)[12,13] can be sensitive to the magnetostatic interaction between magnetic textures, in this case vortex in dots. FORC analysis was developed for geomagnetism[14,15,16] but since then, it has been applied in a wide variety of applications from fine nanoparticles[15,17] and permanent magnets[18,19], to nanodot[20,21], antidots[22,23], other matrices[24,25,26] and thin films[27]. In all the previous studies where FORC was used to characterize arrays of nanoelements, the study disentangled the dipolar interaction of the nanoelements, obtaining valuable information such as the average coercivity or the distribution of switching fields. Crucially, when the nanoelements host magnetic textures and these textures interact with each other, this interaction should leave a footprint in the FORC Diagram, which could be extremely useful for the magnetic characterization of the large array.

Here, we provide a comprehensive study of how to read the interaction between vortexes in the FORC Diagram (FD) and their transit from individual behaviour to collective behaviour where the curl of the magnetization comprises several dots. With the help of micromagnetic simulations, we confirm our experimental interpretation and open the door to future studies where the complex interactions of magnetic textures within large arrays can be unlocked with an easily accessible experimental technique such as the FORC Diagram.

All samples were deposited on a Si substrate with a thermal $SiO_2$ layer of 25nm. An array of dots 200 nm in diameter over a total area of 3×3 $mm^2$ was defined with a CRESTEC e-beam lithography tool and the magnetic dots were deposited by magnetron sputtering with the structure Cr(1)/Py(30)/Pt(2) with the number between brackets the thickness in nanometres and being Py Permalloy (NiFe 81/19%)[28]. The pitch between dots will vary from sample to sample from 600 nm down to 250 nm, where the dots are nearly in contact.

FORCs were acquired with an AGFM[29] (PMC MicroMag 2900 series) at room temperature with the magnetic field applied in-plane to the dots. The procedure to obtain a set of FORCs begins by saturating the sample at a field $H_{sat}$. Then, the field is reduced to the reversal field $H_r$, which serves as the starting point for each FORC. The field is then increased back to positive saturation while measuring the magnetization for every field $H$ in small steps. This protocol is repeated for

all $H_r$ from $+H_{sat}$ to $-H_{sat}$. Once measured, the curves are arranged in a two-dimensional magnetization matrix $M(H, H_r)$ from which the FD is obtained as usual[30]:

$$\rho(H, H_r) = -\frac{1}{2}\frac{\partial^2 M(H,H_r)}{\partial H \partial H_r} \qquad [1]$$

For non-interacting dots, we will use the FD represented in the $(H, H_r)$ coordinate system, while for interacting dots, we will discuss the results in the $(H_c, H_u) = ([H - H_r]/2\,, [H + H_r]/2)$ coordinate system, which is better for comparing our findings with previous studies.

We begin by investigating the array of non-interacting dots, with a sample filled with dots 200 nm in diameter and separated by 600 nm (pitch). As the distance between dots is larger than the diameter, the magnetostatic interaction between dots can be assumed negligible. Fig. 1a shows an SEM picture of the regular array of dots and Fig. 1b shows an MFM image of the relaxed magnetization state of the sample. The dots are in a vortex state with a distinctive core with out-of-plane magnetization (up or down) and curling in-plane magnetization around the core.

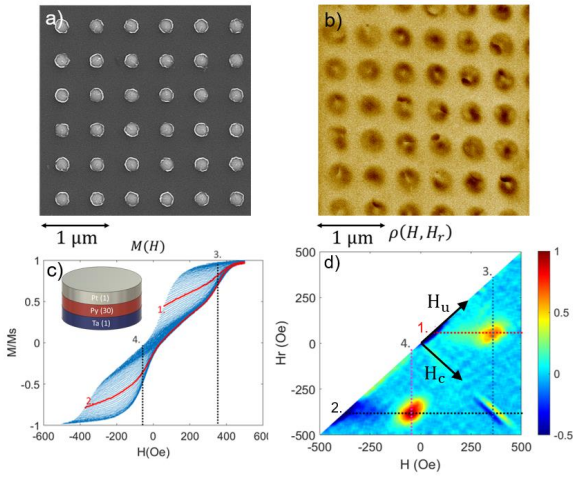


**FIG 1.** (a) SEM image of the array of Py dots with 600 nm pitch. (b) Corresponding MFM image of the same array, obtained with a Park XE7 AFM- MFM using a Cobalt coated cantilever NANOSENSORS PPP-MFMR (c) Minor loops performed to build the FORC Diagram (FD) and the structure of the dot in the inset (d) Corresponding FORC Diagram of the structure. The different lines highlighted in (c) and (d) are guides to the eye to facilitate the discussion in the main text.

Fig.1c shows the minor loops used to build the FD. The double loop, with small coercivity and remanence in the centre, is typical of vortex nucleation in dots[31,32]. Around $H = 0$, most of the dots are in the vortex state (as shown in Fig.1b) and, therefore, the remanence is very small as the sample has roughly equal magnetization pointing in both directions. Then, a large magnetic field is required to annihilate the vortex in all the dots, which broadens the loops in the two lobes at higher fields. The corresponding FD is displayed in Fig. 1d. Two features are visible at $(H, H_r)$ =(-50,-381) Oe with amplitude $\rho(H, H_r) = 0.95$ and at $(H, H_r)$ =(352,44) Oe with amplitude $\rho(H, H_r) = 0.9$, corresponding to the nucleation and annihilation fields respectively. Noticeably, the value $|H_r|$ in the nucleation feature is 29 Oe larger than the value $H$ in the annihilation feature (they are not symmetric to the coercivity diagonal). This fact reflects two different annihilation mechanisms that depend on the return field $H_r$. If the field $H$ is decreased from positive saturation, the vortex nucleates at one edge of the dot, on average around H=+50

Oe, which is the zone of larger susceptibility in the loop. As the field decreases past zero towards negative values, the vortex is pushed towards the side of the dot opposite to the one in which it was nucleated, until it gets annihilated. The situation is different if $H_r$ is positive (highlighted by curve '1' in Fig. 1c). In this case, by decreasing $H$ from positive saturation to $H = +H_r$, a vortex nucleates on one side of the dot but then, by increasing the field $H$ back towards positive saturation in the minor loop, the vortex moves back towards the same side of the dot in which it was nucleated, where it gets annihilated. The FD is also sensitive to the cases in which these two annihilation mechanisms are slightly different (due to any reason such as having an asymmetric shape of the dot or a non-evenly distributed grain distribution, etc.) through the double feature visible at $(H, H_r)$ =(360,-360) Oe in Fig. 1d. This feature is sometimes referred as the 'Butterfly feature[12] and is positioned at H=360 Oe, which is the average annihilation field when the field is cycled from saturation to saturation. At the end of the article, we expand on why this feature appears only if the two annihilation mechanisms are different.

In the FD, we can also notice that the nucleation feature at $(H, H_r)$ =(-50,-381) Oe has a larger intensity $\rho(H, H_r)$ than the annihilation feature at $(H, H_r)$ =(352,44) Oe. As the annihilation feature is built out of minor loops that reflect the movement of the vortex towards annihilation, the fact that this feature is less intense must be related to the 'mobility' of the vortex within the dot. For instance, in a hypothetical case in which the vortex is strongly pinned to the microstructure and it cannot move at all, any minor loop after the vortex nucleation, would be horizontal ($M \sim \text{const}$) until the annihilation field is reached, producing a sudden jump in the loop. In this case, the annihilation feature in the FD would be very sharp, showing a large intensity, $\rho(H, H_r)$. In the opposite case in which the vortex could move at ease without any pinning, any minor loop after nucleation would show a gradual increase in $M$, until the annihilation field is reached. This would result in a distributed annihilation feature with lower intensity, $\rho(H, H_r)$. This interpretation of the meaning of the intensity of the annihilation feature is confirmed experimentally and with micromagnetic simulations in this manuscript.

To provide a qualitative magnitude of how distributed the annihilation feature is, we compare its intensity $\rho(H, H_r)$, with the intensity of the nucleation feature, which should always be sharp because there is little dispersion in the energy required to nucleate the vortex. Therefore, we define the 'asymmetry ratio' $R$ as

$$R = \frac{\rho_A(H,H_r)}{\rho_N(H,H_r)} \quad [2]$$

The superscript 'N' refers to the Nucleation feature (the one at the bottom), and the superscript 'A' refers to the Annihilation feature (the one at the top). Large asymmetry ratios $R$ (sharp nucleation and annihilation feature) imply that local interactions impede the vortex movement.

For instance, using polycrystalline Co dots instead of Py dots, we expect larger vortex pinning (i.e. lower vortex mobility) due to the stronger anisotropy in Co. Suppl. Info. Fig.S1 shows the experimental FD for Co dots with the same diameter and pitch as the Py dots shown in Fig.1a (D=200 nm, Pitch=600 nm). The asymmetry ratio for Co is $R_{Co} = 0.86$, while in the case of Py (Fig. 1d) is $R_{Py} = 0.68$. Indeed, a larger value of $R$ in Co dots indicate the lower vortex mobility. Additionally, if the size of the dots is reduced, one can also intuitively expect a reduced mobility of the vortex due to the geometric constriction of the small dot. We have checked this point with micromagnetic simulations (see details of the Mumax3[33] micromagnetic simulation in Suppl. Info. S1), extracting the asymmetry ratio in non-interacting Py dots of different diameters. As shown in Suppl. Info. Fig. S2, the smaller the dot, the larger the value of $R$, due to the reduced mobility of the vortex in smaller dots. The two examples mentioned in this paragraph reinforce the correctness of our interpretation of the 'asymmetry ratio' $R$.

After disentangling the main features of the FD in non-interacting dots, we now discuss how these features change in the more interesting case of interacting dots. Fig. 2 shows the FD for Py dots with the same diameter of 200 nm but different pitch, ranging from 500 nm to 200 nm. Note that pitch 600 nm is shown in Fig. 1d. The FDs in Fig. 2 show that the nucleation and the annihilation features get closer to each other as the distance between the dots decreases until they eventually collapse to one sharp feature at $H = H_r = 0$, which resembles the FD of a uniform Permalloy thin film with small coercivity.

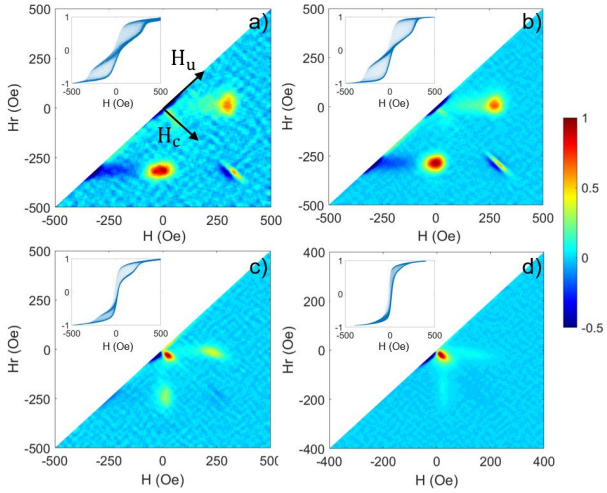


**FIG 2.** FORC diagrams for arrays of Py dots 200 nm in diameter and with 500 nm pitch (a), 400 nm pitch (b), 300 nm pitch (c) and 250 nm pitch (d).

As explained in the introduction, in the FORC diagram, the interactions within a ferromagnetic system are often discussed in terms of the coercive $H_c$ and bias $H_u$ axis, represented by black arrows in Fig. 2a and defined as $(H_c, H_u) = ([H - H_r]/2\,, [H + H_r]/2)$. In these coordinates, the value $H_u$ of each feature reflects how much the local interactions affect the magnetization process. In Fig.3a, we plot the difference in the $H_u$ value for the Nucleation $H_u^N$ and the annihilation feature $H_u^A$, $\Delta H_u = H_u^N - H_u^A$, together with the asymmetry ratio $R$, defined by the expression [2], as a function of the distance between dots or pitch. As visible in Fig. 3a, the experimental $\Delta H_u$ (red circles) decreases significantly when the pitch decreases (and their magnetostatic interaction increases). The decrease of $\Delta H_u$ is somehow surprising because an enhanced interaction between objects is usually associated with an *increase* of the width of the corresponding feature in the FD along the $H_u$ axis[34,35], in clear contrast with our results. In parallel, the asymmetry ratio $R$ (black circles in Fig. 3a) has a roughly constant value for large pitch but experiences a prominent increase to values larger than one for small pitch. If $R>1$, the annihilation feature is sharper than the nucleation feature, which is the opposite of what we find for large pitch and non-interacting dots, and it should reflect that the interaction between dots is promoting the vortex annihilation in individual dots.

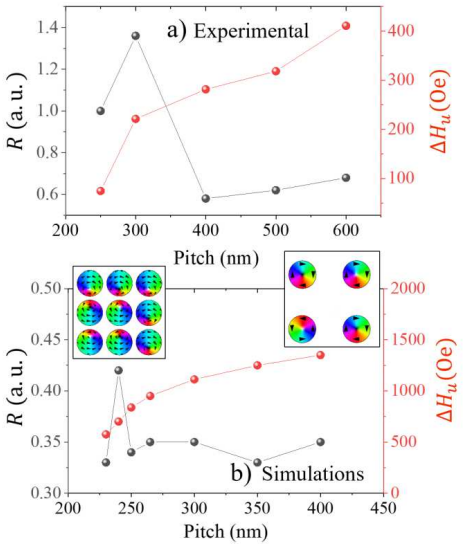


**FIG. 3.** (a) Asymmetry Ratio $R$, defined by expression [2], and $\Delta H_u$ extracted from Fig.2 for the experimental samples. (b) Asymmetry Ratio $R$ and $\Delta H_u$ extracted from micromagnetic simulations of 200 nm diameter dots. The cartoons in (b) represent an isolated vortex in each dot for a large pitch (cartoon on the right) and a vortex texture comprising several dots (cartoon on the left) when the pitch is small and the interaction between dots increases.

To confirm this interpretation, in Fig. 3a we have performed micromagnetic simulations on 200 nm diameter dots and variable separation between the dots. Fig. 3b shows the asymmetry Ratio $R$ and $\Delta H_u$ obtained from micromagnetic simulations (the corresponding FD from the simulation can be found in Suppl. Info. S3). The simulated $\Delta H_u$ values are larger than the experimental ones because the simulation was performed at 0K. In the simulation, at a pitch smaller than 250 nm, the vortices in individual dots begin to interact with each other magnetostatically. At this pitch, there is a sudden increase in the value of $R$, in parallel with a change in the slope of $\Delta H_u$. The magnetostatic interaction between dots promotes the vortex annihilation in the individual dots, favouring collective curling of the magnetization covering several dots. This multi-dot vortex texture has been experimentally observed before, using optical techniques[36] and, as we have shown, it can also be inferred from the FD.

Finally, we turn our attention to the butterfly feature. This feature was present in all the experimental FDs shown in this work, using Permalloy or Cobalt. On the other hand, the micromagnetic simulations on circular Permalloy dots do not produce the butterfly feature as shown in Fig. 4a, despite a considerable effort trying several options with the crystalline structure and the magnetic anisotropy. On the other hand, if we introduce a small notch on one of the sides of the dot (Fig. 4b), this asymmetry does produce a butterfly feature in the simulated FD (marked by an arrow in Fig. 4b). This is a strong indication that the butterfly feature appears when the mechanism of vortex annihilation is different if the vortex is annihilated on the same side of the dot in which it was nucleated or on the opposite side of the dot. Indeed, if the defect in the dot is symmetric to the path that the vortex follows from nucleation to annihilation (Fig. 4c), the butterfly feature in the simulation disappears again.

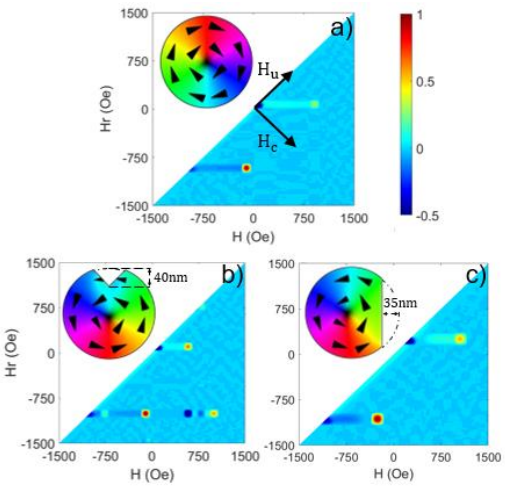


**FIG. 4.** FORC diagram simulated for a Py dot 200 nm in diameter (a), for the same dot with a notch on one of the sides (b) and for a defect that runs along the path the vortex follows from nucleation to annihilation (c).

In conclusion, in this work, we have used a FORC diagram to characterize the magnetization process in a large array of circular ferromagnetic dots. We have described the features in the FD that mark the onset of vortex nucleation and annihilation and how their position can vary from material to material, providing a tool to interpret the magnetization process in large arrays of nanoelements, even if they are made of different materials. The asymmetry ratio $R$, defined by expression [2], is a signature of the vortex mobility within the dot and can also indicate an inter-dot vortex collective interaction when the structures are in proximity. Finally, we have shown that the butterfly feature appears when the different vortex annihilation paths are not equivalent. Although the specific cause of this asymmetry may not be easy to discern without extensive micromagnetic simulations, it is a quick indication of a particular behaviour that may be relevant in spin-ice structures dedicated to neuromorphic behaviour.

We should emphasize the importance of having an experimental method to characterize the average individual behaviour of nanostructures in a large array, which may not be achievable with other experimental techniques. The details in the FD must be initially understood with the help of micromagnetic simulations but, once this is done, the FD diagram can be the sole characterization technique in samples with variations of the same array of nanostructures. Therefore, we believe the FORC diagram may become a pivotal experimental technique to characterize large arrays of nanostructures, which are key in emerging fields such as neuromorphic computing.

**Supplementary material**

We included two supplementary subsections to support the main text. Subsection S1 provides evidence for the interpretation of the asymmetry factor R, including: (FIG. S1) the FORC diagram for a cobalt nanodot array with the same geometry as in the first permalloy sample, and (FIG. S2) micromagnetic simulations of R in single permalloy dots with decreasing diameter. Subsection S2 presents the simulated FORC diagrams (FIG. S3) corresponding to Fig. 3b.

**Acknowledgements**

This work received funding from the Spanish Ministry of Science and Innovation through projects: PID2020-117024GB-C4, PID2020-117024GB-C41 and PID2023-150853NB-C32. The authors acknowledge Prof. C. Aroca for fruitful discussions and ICTS Micronanofabs.

**References**

[1] S.H. Skjærvø, C.H. Marrows, R.L. Stamps and L.J. Heyderman, "Advances in artificial spin ice", Nat Rev Phys **2**, 13 (2020).
[2] E. Mengotti, L. Heyderman, A. Rodríguez, F. Nolting, R.V. Hügli and H-B. Braun, "Real-space observation of emergent magnetic monopoles and associated Dirac strings in artificial kagome spin ice", Nature Phys. **7**, 68 (2011).
[3] M.J. Morrison, T.R. Nelson and C. Nisoli, "Unhappy vertices in artificial spin ice: new degeneracies from vertex frustration", New J. Phys. **15**, 045009 (2013).
[4] S. Gliga, G. Hrkac, C. Donnelly, J. Büchi, A. Kleibert, J. Cui, A. Farhan, E. Kirk, R.V. Chopdekar, Y. Masaki, N.S. Bingham, A. Scholl, R.L. Stamps and L.J. Heyderman, "Emergent dynamic chirality in a thermally driven artificial spin ratchet", Nature Mater. **16**, 1106 (2017).
[5] M. Krawczyk and D. Grundler, "Review and prospects of magnonic crystals and devices with reprogrammable band structure", J. Phys. Condens. Matter **26**, 123202 (2014).
[6] J.C. Gartside, K.D. Stenning, A. Vanstone, H.H. Holder, D. M. Arroo, T. Dion, F. Caravelli, H. Kurebayashi and W. R. Branford, "Reconfigurable training and reservoir computing in an artificial spin-vortex ice via spin-wave fingerprinting", Nat. Nanotechnol. **17**, 460 (2022).
[7] D. Suess, A. Bachleitner-Hofmann, A. Satz, H. Weitens- felder, C. Vogler, F. Bruckner, C. Abert, K. Pru¨gl, J. Zimmer, C. Huber, S. Luber, W. Raberg, T. Schrefl and H. Brückl, "Topologically protected vortex structures for low-noise magnetic sensors with high linear range", Nat. Electron. **1**, 362 (2018).
[8] S. Wintz, V. Tiberkevich, M. Weigand, J. Raabe, J. Lindner, A. Erbe, A. Slavin and J. Fassbender, "Magnetic vortex cores as tunable spin-wave emitters", Nat. Nanotechnol. **11**, 948 (2016).
[9] H. Yu, J. Chen, V. Cros, P. Bortolotti, H. Wang, C. Guo, F. Brandl, F. Heimbach, X. Han, A. Anane and D. Grundler, "Active Ferromagnetic Metasurface with Topologically Protected Spin Texture for Spectral Filters", Advanced Functional Materials **32**, 34 (2022).
[10] J. Torrejon, M. Riou, F. A. Araujo, S. Tsunegi, G. Khalsa, D. Querlioz, P. Bortolotti, V. Cros, K. Yakushiji, A.Fukushima, H. Kubota, S. Yuasa, M. D. Stiles and J. Grollier, "Neuromorphic computing with nanoscale spintronic oscillators", Nature **547**, 428 (2017).
[11] M. Romera, P. Talatchian, S. Tsunegi, F. A. Araujo, V. Cros, P. Bortolotti, J. Trastoy, K. Yakushiji, A. Fukushima, H. Kubota, S. Yuasa, M. Ernoult, D. Vodenicarevic, T. Hirtzlin, N. Locatelli, D. Querlioz and J.Grollier,"Vowel recognition with four coupled spin- torque nano-oscillators", Nature **563**, 230 (2018).
[12] C. R. Pike, A. P. Roberts, and K. L. Verosub, "Characterizing interactions in fine magnetic particle systems using first order reversal curves", J. Appl. Phys. **85**, 6660 (1999).
[13] A. P. Roberts, C. R. Pike, and K. L. Verosub, "First-order reversal curve diagrams: A new tool for characterizing the magnetic properties of natural samples", J. Geophys. Research: Solid Earth **105**, 28461 (2000).
[14] C. Carvallo, O. Ozdemi, and D. J. Dunlop, "First-order reversal curve (FORC) diagrams of elongated single- domain grains at high and low temperatures", J. Geophys. Research: Solid Earth **109**, B04105 (2004).
[15] C. R. Pike, A.P. Roberts, and K. L. Verosub, "First-order reversal curve diagrams and thermal relaxation effects in magnetic particles", Geophys. J. International **145**, 28461 (2001).
[16] A. R. Muxworthy, J. G. King, and D. Heslop, "Assessing the ability of first-order reversal curve (FORC) diagrams to unravel complex magnetic signals", Journal of Geophysical Research **110**, B01105 (2005).
[17] C. Carvallo, A. R. Muxworthy, and D. J. Dunlop, "First- order reversal curve (FORC) diagrams of magnetic mixtures: Micromagnetic models and measurements", Physics of the Earth and Planetary Interiors **154**, 308 (2006)
[18] S. Ilse, F. Groß, J. Gräfe, and E. Goering, "Understanding the interaction of soft and hard magnetic components in NdFeB with first-order reversal curves", Phys. Rev. B **103**, 024425 (2021).

[19] H. Chiriac, N. Lupu, L. Stoleriu, P. Postolache, and A. Stancu, "Experimental and micromagnetic first-order reversal curves analysis in NdFeB-based bulk 'exchange spring' type permanent magnets", J. Mag. Mag. Mat. **316**, 177 (2007).
[20] C. Pike and A. Fernandez, "An investigation of magnetic reversal in submicron-scale Co dots using first order reversal curve diagrams", J. Appl. Phys. **85**, 6668 (1999).
[21] R. K. Dumas, C. P. Li, I. V. Roshchin, I. K. Schuller, and K. Liu, "Magnetic fingerprints of sub- 100 nm Fe dots", Phys. Rev. B **75**, 134405 (2007).
[22] J. Gräfe, M. Weigand, C. Stahl, N. Träger, M. Kopp, G. Schütz, E. J. Goering, F. Haering, P. Ziemann, and U. Wiedwald, "Combined first-order reversal curve and x-ray microscopy investigation of magnetization reversal mechanisms in hexagonal antidot lattices", Phys. Rev. B **93**, 014406 (2016).
[23] J. Gräfe, M. Weigand, N. Träger, G. Schütz, E. J. Goering, M. Skripnik, U. Nowak, F. Haering, P. Ziemann, and U. Wiedwald, "Geometric control of the magnetiza- tion reversal in antidot lattices with perpendicular magnetic anisotropy", Phys. Rev. B **93**, 104421 (2016).
[24] M. P. Proenca, K. J. Merazzo, L. G. Vivas, D. C. Leitao, C. T. Sousa, J. Ventura, J. P. Araujo, and M. Vazquez, "Co nanostructures in ordered templates: Comparative FORC analysis", Nanotechnology **24**, 475703 (2013).
[25] M. P. Proenca, C. T. Sousa, J. Ventura, J. García, M. Vazquez, and J. P. Araujo, "Identifying weakly-interacting single domain states in Ni nanowire arrays by FORC", Journal of Alloys and Compounds **699**, 421 (2017).
[26] C. Martín-Rubio, A. Rivelles, M. Schneider, J. C. del Hoyo, V. Privitera, M. Worgull, M. Maicas, R. Sanz, "Magnetic Characterization of Permalloy Nanodome Surfaces on Flexible PEEK/TiO2 Vertical Nanotubes Composites", IEEE Transactions on Magnetics **59**, 2 (2023).
[27] Z. Ferhat, A. Rivelles, M. Abuín, R. Guedas, and J. L. Prieto, "Magnetic and magnetoresistive characterization of a top-pinned spin-valve with a multilayer with perpendicular-to-plane anisotropy deposited on top", J. Appl. Phys. **134**, 233905 (2023).
[28] A. Rivelles, "Fabrication and characterization of magnetic devices: From space applications to spintronics", Doctoral thesis, Universidad Politécnica de Madrid, E.T.S.I. Telecomunicación (2024).
[29]P. Flanders, "An alternating-gradient magnetometer", J. Appl. Phys. **63**, 3940 (1988).
[30] A. R. Muxworthy and A. P. Roberts, "First-order reversal curve (FORC) diagrams", Encyclopaedia of Geomagnetism and Palaeomagnetism, Springer, p. 266, (2007).
[31] M. Goiriena-Goikoetxea, K. Y. Guslienko, M. Rouco, I. Orue, E. Berganza, M. Jaafar, A. Asenjo, M. L. Fernández-Gubieda, L. Fernández Barquíng and A. García-Arribas, "Magnetization reversal in circular vortex dots of small radius", Nanoscale **9**, 11269 (2017).
[32] M. Galvis, F. Mesa, J. Restrepo, "Micromagnetic behavior of permalloy (Ni80Fe20) nanodots as a function of aspect ratio", Comp. Mat. Sci. **245**, 113330 (2024).
[33] A. Vansteenkiste, J. Leliaert, M. Dvornik, M. Helsen, F. Garcia-Sanchez, and B. Van Waeyenberge, "The design and verification of MuMax3", AIP Advances **4**, 107133 (2014).
[34] V.M. Andrade, S. Caspani, A. Rivelles, S. A. Bunyaev, V.O. Golub, J.P. Araujo, G.N. Kakazei, C.T. Sousa, M.P. Proenca, "Bilayered soft/hard magnetic nanowires as in-line writing heads", Materials and Design **222**, 111024 (2022).
[35] C-I Dobrotă, A. Stancu, "What does a first-order reversal curve diagram really mean? A study case: Array of ferromagnetic nanowires". J. Appl. Phys. **113**, 043928 (2013).
[36] M. Natali, A. Popa, U. Ebels, Y. Chen, S. Li, M. E. Welland, "Correlated vortex chiralities in interacting Permalloy dot patterns", J. Appl. Phys. **96**, 4334 (2004).